Geomorphology 290 (2017) 265–276

Contents lists available at ScienceDirect

Geomorphology

journal homepage: www.elsevier.com/locate/geomorph

Shoreline resilience to individual storms and storm clusters on a meso-macrotidal barred beach

Donatus Bapentire Angnuureng[a,b,c,*], Rafael Almar[b], Nadia Senechal[a], Bruno Castelle[a], Kwasi Appeaning Addo[c], Vincent Marieu[a], Roshanka Ranasinghe[d,e,f]

[a] UMR EPOC, University of Bordeaux/CNRS, Bordeaux, France
[b] UMR LEGOS, University of Toulouse/CNRS/IRD/CNES, Toulouse, France
[c] MAFS/Remote Sensing Laboratory, University of Ghana, Accra, Ghana
[d] UNESCO-IHE, Delft, The Netherlands
[e] Harbour, Coastal and Offshore Engineering, Deltares, Delft, The Netherlands
[f] University of Twente, Enschede, The Netherlands

ARTICLE INFO

Keywords:
Storm clusters
Beach erosion and recovery
Sandbar
Extreme events impact
Open beach
Short-term morphodynamics

ABSTRACT

This study investigates the impact of individual storms and storm clusters on shoreline recovery for the meso-to macrotidal, barred Biscarrosse beach in SW France, using 6 years of daily video observations. While the study area experienced 60 storms during the 6-year study period, only 36 storms were analysed due to gaps in the video data. Based on the 36 individual storms and 13 storm clusters analysed, our results show that clustering impact is cumulatively weak and shoreline retreat is governed by the first storms in clusters, while the impact of subsequent events is less pronounced. The average post-storm beach recovery period at this site is 9 days, consistent with observations at other beaches. Apart from the dominant effect of present storm conditions, shoreline dynamics are also significantly affected by previous storm influence, while recovery is strongly modulated by tidal range and the bar location. Our results reveal that not only is the storm energy important but also the frequency of recurrence (storms result in greater retreat when time intervals between them are longer), which suggests an interaction between short storm events and longer-term evolution.

1. Introduction

Sustainable management of coastal resources requires a thorough understanding of the processes that drive changes in the shoreline location. The shoreline is a highly dynamic interface between land and ocean and is thus affected by various forces operating at different spatio-temporal scales. Shoreline evolution is to a large extent governed by meteorological and oceanic conditions: waves, tides, currents and atmospheric conditions (wind, inverse barometer). It is generally assumed that wave breaking is the main driver of coastal evolution but its role may be strongly modulated by other factors. For example, on the lower part of the beach (the beach margin beneath the water surface from the shoreline), a storm may have more erosive impact at low tide than at high tide. Although many studies have focused either on simple or complex paradigms of shoreline evolution from Wright and Short's (1984) beach state classification method, as well as more complex cross-shore equilibrium models (Yates et al., 2009) and a mix of cross-and alongshore-based models (Morton et al., 1993; Hansen and Barnard, 2010), the response to perpetually changing forcing conditions is still somewhat unclear (Ranasinghe et al., 2012; Pianca et al., 2015). The fact that beaches eventually recover to their pre-storm state means that the beach response does not only depend on storm conditions but also on other factors such as sea level and its chronic behavior (Zhang et al., 2002), the previous beach state (Wright et al., 1985; Grasso et al., 2009; Yates et al., 2009) and/or previous wave conditions (Davidson et al., 2013; Splinter et al., 2014b).

Given that individual storms can result in dramatic shoreline changes, storms can be treated as outliers (Zhang et al., 2002). Despite their large impact, storms are considered independent from long-term evolution and described separately because of their transient influence due to rapid post-storm recovery. Zhang et al. (2002) support the assertion of Douglas and Crowell (2000) that the most practical option is to remove such events from long-term evolution studies. In contrast, Fenster et al. (2001) and Genz et al. (2007) observed that individual storms should not be excluded, and that including their contribution could potentially improve the prediction of long-term shoreline evolution. The short-term shoreline changes induced by storms are generally characterized by a rapid erosion followed by a slower post-storm

* Corresponding author at: UMR EPOC, University of Bordeaux/CNRS, Bordeaux, France.
E-mail address: donatus.angnuureng@ucc.edu.gh (D.B. Angnuureng).

http://dx.doi.org/10.1016/j.geomorph.2017.04.007
Received 7 August 2015; Received in revised form 24 February 2017; Accepted 6 April 2017
Available online 09 April 2017
0169-555X/

recovery and are influenced by storm characteristics (e.g. energy and duration, individual versus sequences of storms, or storm clusters; see, among others, Yates et al., 2009; Karunarathna et al., 2014; Coco et al., 2014; Senechal et al., 2015).

Investigations on storm impact have mainly followed two approaches; 1) non-cumulative analyses (e.g. Frazer et al., 2009; Coco et al., 2014; Splinter et al., 2014a) which take individual storms as independent events and show that frequent storms or storm sequences do not have a persistent influence on longer term shoreline evolution and; 2) cumulative storms analysis (e.g. Ferreira, 2005; Karunarathna et al., 2014) which shows that storm sequences enhance erosion. The latter has been further evidenced recently by equilibrium-based semi-empirical shoreline models (e.g. Yates et al., 2009; Davidson et al., 2013; Castelle et al., 2014) with the rate of shoreline migration under a storm depending on the disequilibrium between the storm energy and previous beach state, and the beach constantly trying to reach a new equilibrium under varying waves. The equilibrium approach raises the importance of the so-called beach 'memory effect' that suggests beach response depends on the antecedent wave conditions. The transient or persistent effects of individual storms and storm clusters is still a subject of debate and discrepancies on storm impact characterization still exist (e.g. Dolan and Davis, 1992; Mendoza et al., 2011; Splinter et al., 2014a; Senechal et al., 2015).

To understand the persistence of storms and beach resilience to different storm recurrence intervals and intensities, a good understanding of post-storm beach recovery conditions and duration is crucial. Beach recovery from storms depends on the severity of the event(s) and on how far the sediment has been transported offshore (Corbella and Stretch, 2012). With high frequency (daily) video data, post-storm recovery durations of 5 to 10 days have been reported by Ranasinghe et al. (2012) for the microtidal Palm beach, Australia and Duck beach, USA. However, the recovery duration is yet to be investigated at high-energy meso- to macrotidal beaches, although Senechal et al. (2015) postulated that recovery at these latter types of beaches could be rapid. This could be due to the presence of 'usual' winter storm conditions. To date, different diagnostics have been used to quantify beach recovery in various studies (e.g. Maspataud et al., 2009; Corbella and Stretch, 2012; Ranasinghe et al., 2012) and an objective means of comparing and contrasting these different estimates is yet to be identified.

Although it is widely accepted that the shoreline is mostly affected by waves, the influence of tidal range and sandbar location cannot be overlooked, in particular at barred meso- to macrotidal beaches such as encountered along the SW France Aquitaine Coast (Castelle et al., 2007a) or at Perranporth in the north-west coast of Cornwall in the UK (Stokes et al., 2015). It has been observed that storm events, while capable of causing large short-term changes in the shoreline, do not singularly account for the overall observed change (Hansen and Barnard, 2010), and wave impact could be negligible with respect to the magnitude of the seasonal signal and the effect of the inter-annual signals (Pianca et al., 2015). In macrotidal environments, tides are regarded as a primary factor in the control of the hydrodynamic and sedimentary processes of intertidal flats (Davis, 1985; Masselink and Short, 1993; Robin et al., 2007). There is field evidence for the tidal modulation (attenuation) of incident wave power by the large tidal range (Robin et al., 2007; Davidson et al., 2008; Guedes et al., 2011) which eventually affects the shoreline. Zhang et al. (2002) observed that the combination of large waves with high water levels during five continuous high tides caused the largest recorded dune (upper beach) erosion from Long Island, New York, to Cape Hatteras. This suggests that the effect of tides actually depends on the part of beach (upper, intertidal or lower) being investigated. However, the effect of tides on storm impact at meso- to macrotidal sandy shorelines is relatively poorly investigated, although some recent studies suggest the inclusion of tidal range in shoreline prediction models can be important (Stokes et al., 2015).

Changes in sandbar location due to varying wave conditions have been widely documented (e.g. Wright et al., 1985; Lippmann and Holman, 1990; Gallagher et al., 1998; Castelle et al., 2007a, among others). Bar decay can result in its inability to offer protection during storms, leading to intensified upper beach erosion (Castelle et al., 2007b), and alongshore irregularities of sandbar crest can force a template of onshore wave field resulting in localized upper beach erosion (Thornton et al., 2007; Castelle et al., 2015). At barred beaches with large tidal ranges, it is observed that both the sandbar and the tide modulate onshore wave breaking intensity and control morphological changes (Almar et al., 2010; Ba and Senechal, 2013; Stokes et al., 2015). Although shoreline and sandbar changes have been studied rather extensively (e.g. Lippmann and Holman, 1990; Hansen and Barnard, 2010; van de Lageweg et al., 2013), changes have been studied mostly as discrete events (except in few studies such as van de Lageweg et al., 2013 at an embayed beach) and their combined effect on storm impact and beach recovery evolution is still uncertain.

The above discussion highlights that there are still many knowledge gaps regarding shoreline resilience to storms at meso- to macrotidal beaches. This study aims to take a first step towards addressing some of these knowledge gaps. Specifically, the objective of this study is to: (a) quantify shoreline resilience to individual storms and storm clusters, (b) investigate the influence of tide and sandbars on shoreline position, and (c) estimate the post-storm beach recovery duration. To achieve this goal, six years (2007–2012) of daily video observations at Biscarrosse, a barred meso- to macrotidal beach, are analysed. In Section 2, the study site and video methods are described. Section 3 presents the results on the shoreline response to storms at timescales from days to years, with an emphasis on the influence of storm recurrence and the modulation played by tidal range and sandbar. The role of tide on shoreline response to storms and the importance of the frequency of recurrence of storms on shoreline resilience are discussed in Section 4 and, finally, conclusions are presented in Section 5.

2. Methods

2.1. Field site

Biscarrosse beach, located in the SW France (Fig. 1), is exposed to long and energetic waves originating mainly from the W-NW. The mean annual offshore significant wave height *Hs* is reported as 1.4 m with an associated averaged mean period T_p of 6.5 s (Butel et al., 2002). Waves show seasonal variability (Butel et al., 2002): during fall and winter seasons (November to March), mean *Hs* is 1.6 m and T_p is 7.3 s, while during spring and summer (April to October) mean *Hs* is 1.1 m with a shorter T_p of 6 s (Senechal et al., 2015). The tidal range is meso- to macrotidal, with an average value of 2.9 m that increases up to 5 m during spring tide. The average beach slope is about 0.03, and sediment at the site consists of fine to medium quartz sand with median grain sizes ranging from 0.2 to 0.4 mm (Gallagher et al., 2011).

Biscarrosse is an open double-barred beach; the outer bar often exhibits crescentic patterns, while the inner bar in the intertidal domain commonly exhibits a transverse bar and rip (TBR) morphology with a mean wavelength of about 400 m (Almar et al., 2010). Based on three years of daily video images, Peron and Senechal (2011) also indicate that both up-state and down-state transitions were dependent on the previous beach state and that no 'direct jump' from the reflective state to the dissipative beach state was observed. They discussed the possibility that the presence of the subtidal bar probably explained the persistence of TBR beach state (mean residence time of about 24 days reaching maximum at 103 days), even during high-energy conditions as reported in other similar environments (Almar et al., 2010). Using three years of video observations, Senechal et al. (2015) showed that the range of variation of the inner sandbar location (120 m) at Biscarrosse is two and a half times larger than the range of variation of the shoreline and that rapid erosion of the shoreline can be observed under moderate conditions.

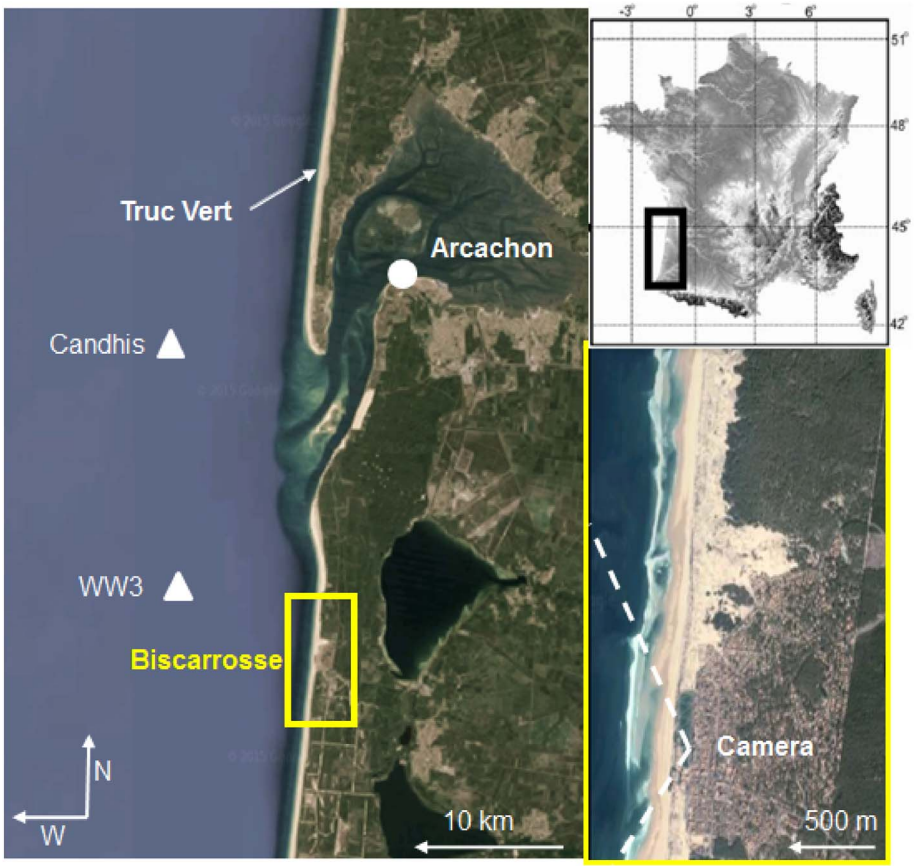

Fig. 1. Location of the study site, Biscarrosse beach (SW France), showing the WW3 grid node (triangle) located at − 1°30′ W, 44°30′ N and Candhis buoy (triangle) at 1°26.8′W, 44°39.15′ N and the video station.

2.2. Video data

A shore-based video system (e.g. Lippmann and Holman, 1989, 1990; Holman et al., 1993; Plant and Holman, 1997) was installed at Biscarrosse beach in April 2007 by EPOC laboratory (CNRS/University of Bordeaux) in collaboration with the New Zealand National Institute of Water and Atmosphere (NIWA) (see Almar et al., 2009; Senechal et al., 2015). The video station contains five color cameras fixed atop the foredune at 26 m above the mean sea level (MSL), although only four camera images (Fig. 2a–d) were in good state during the observation period of the present study. The system provides three types of images every 15 min including processing time: snapshot, cross-shore time stacks and 10-min time exposure (or timex) images. Images are merged and rectified on a 1 m × 1 m grid using conventional photogrammetric methods (Holland et al., 1997). The transformation between oblique image and real-world coordinates was achieved using 18 ground control points surveyed with a differential GPS (DGPS, centimeter accuracy). The origin (X = 0, Y = 0) of the local coordinate system is the camera location oriented along the cross-shore (X) and alongshore (Y) directions while the vertical Z = 0 origin denotes the Mean Sea Level (MLS). A region covering beach area of 1200 m alongshore and 400 m cross-shore is observed (Fig. 2e, f).

Commonly used proxies for shoreline position are either based on visual assessment (e.g. the high water line) or datum-based (see Boak and Turner, 2005). Datum-based shorelines generally consist of the cross-shore position of a specified elevation contour, such as mean high water (MHW), the method chosen in this study. Shorelines derived from video have become increasingly common (Plant and Holman, 1997; Aarninkhof et al., 2003; Plant et al., 2007; Smit et al., 2007). Different categories of images have been used to delineate shoreline, with the first methods based on gray images (Plant and Holman, 1997; Madsen and Plant, 2001) being the popular SLIM method, a typical approach where an intensity peak is used as a proxy for the location of the shoreline, and suitable for reflective beaches (Plant et al., 2007). Subsequent methods used color images (or both color and gray), a more sophisticated method (Turner et al., 2001; Aarninkhof et al., 2003) based on color segmentation, applicable to detecting the shoreline at both reflective and dissipative beaches. In our study, errors have been minimized with the manual delineation of the shoreline (Fig. 2e) to ensure a high-quality dataset. At meso- to macrotidal barred beaches, it is difficult to select the elevation that best represents the overall intertidal complex morphology, as observed by Castelle et al. (2014). Following this and to minimize the influence of the complex intertidal zone, shoreline location was defined here for elevations at 0.45 m ± 0.1 m above MSL (Fig. 2) which corresponds to the lowest high tide level, commonly used through video imagery to get daily shoreline data at meso- to macrotidal beaches (e.g. Birrien et al., 2013; Senechal et al., 2015). Due to the absence of a tide gauge at Biscarrosse, the tide used here was extracted from a reconstructed tidal signal based on tidal harmonics (WXtide software, Flater, 2010) with reference to the closest point at Arcachon (1°10 W, 44°40 N, Fig. 1), about 30 km from Biscarrosse (after phase-lag correction). Overall, the video-derived shoreline dataset covers 1036 days in 6 years, which is 54.2% of the study period.

Video-derived shorelines are subject to relatively large uncertainties (Holman and Stanley, 2007). In particular, the shoreline-detection methods are sensitive to waves and lighting conditions. For instance, the SLIM method by Plant and Holman (1997) is sensitive to variations in water levels which can scale the effects of both setup and run-up, and fog can reduce the color signal strength (Aarninkhof et al., 2003). However, the results of shoreline measured from video have been comparable to that of topographic surveys (Holman and Haller, 2013)

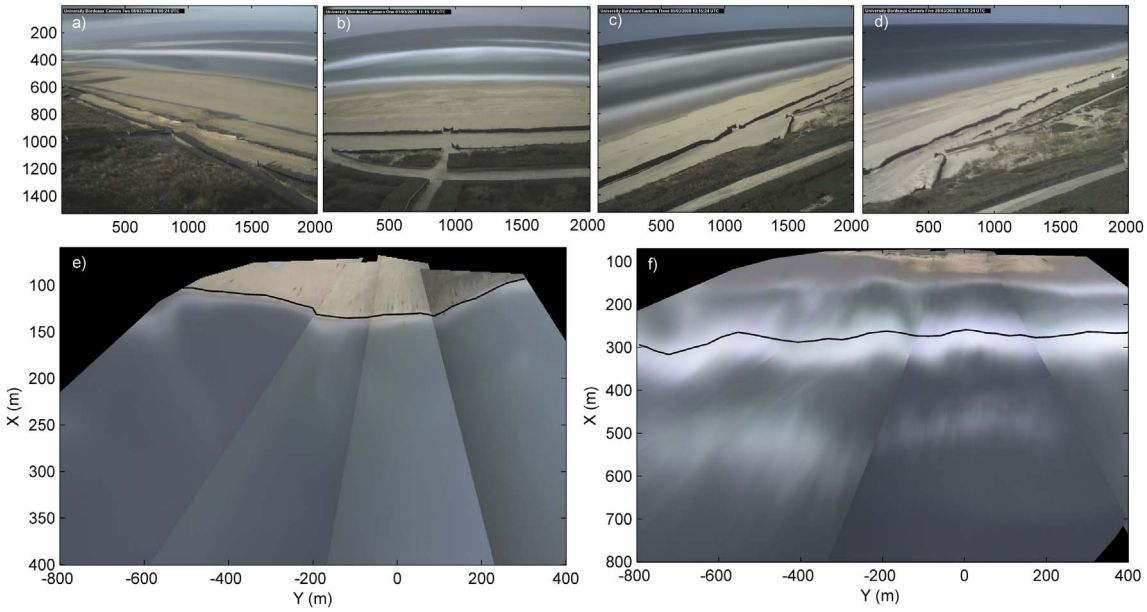

Fig. 2. Illustration of camera view fields (a-d) from oblique 10-min averaged images with manual delineation of e) shoreline (29 Sept. 2008) and f) inner sandbar crest (15 June 2007) on rectified, merged images.

and the differences have been extensively discussed in previous works (e.g. Aarninkhof et al., 2003; Plant et al., 2007). In addition to the error related to image rectification estimated here at 1–2 m, an error of 0.5 m is added for shoreline identification equal to the pixel footprint. The mean pixel resolution at the shoreline location is about 0.1 m and 0.2 m in the cross-shore and alongshore directions, respectively, which worsen to 1–3 m at the viewed edges. Due to the lack of information on the actual surf zone bathymetry, the main horizontal uncertainty, the wave-induced setup was estimated at $0.35\beta\sqrt{HsL}$, with β the upper beach slope and L the offshore wave length, following Stockdon et al. (2006). Aarninkhof et al. (2003) reported that such simplification introduces minor deviations in the wave-induced setup at the shoreline. The associated setup error on shoreline location is about 6 m (for $Hs \sim 6$–8 m) considering the average beach slope of 0.03, but ranges between 2 and 12 m for all the data. For complex submerged morphological beaches such as Biscarrosse, alongshore variations of wave-induced setup can be established. In our study, this bias is substantially reduced because shoreline location is estimated out of stormy periods. Given the restraints listed above, we estimate that the overall uncertainty on video-derived shoreline location is about 9 m.

Timex images (Fig. 2f) are used, to average-out high-frequency intensity fluctuations due to individual waves, providing a statistically stable pattern of the breaking (Lippmann and Holman, 1989; van Enckevort and Ruessink, 2001). The high-intensity bands associated with breaking (see Fig. 2f) are commonly used as a proxy for bar crest location (Lippmann and Holman, 1989; Pape and Ruessink, 2008; Almar et al., 2010; Guedes et al., 2011). There is always a substantial error O (1–10 m) when locating the cross-shore position of the bar crests (van Enckevort and Ruessink, 2001). This is mostly due to the translation of the breaking zone resulting from the changes in wave characteristics and tidal level (Lippmann and Holman, 1989; van Enckevort and Ruessink, 2001). In order to reduce the differences between the detected and actual bar crest locations, and to be consistent with previous methodologies (e.g. van de Lageweg et al., 2013; Senechal et al., 2015) images for which $Hs > 2.5$ m were discarded. Inner-bar extraction was done at a constant water level of 0.55 ± 0.1 m below MSL. The detection resulted in 411 daily alongshore-averaged cross-shore sandbar positions $< X_b >$ or lines, which is 20% of the entire period.

The reason for choosing low tide to pick the sandbar location relates to the fact that waves barely break over the inner bar at high tides for intermediate to fair energetic conditions. Several studies have shown that surveyed sandbar crests and those extracted from timex video images are in good agreement ($R^2 \sim 0.8$; Lippmann and Holman, 1989; Plant and Holman, 1998). The accuracy of sandbar location also depends on the rectification error of 1–2 m and due to manual digitization and the pixel footprint of 2 m, tide- and wave-induced artificial shift (van Enckevort and Ruessink, 2001; Pape and Ruessink, 2008; Almar et al., 2010) of 5–10 m. In the sandbar location, the pixel footprint was poorer (reaching 12 m) at around 400 m from the camera. Considering all of the above-mentioned sources of uncertainty, an overall error of 15 m for the sandbar location is calculated for this site, consistent with that reported at Truc Vert beach (Almar et al., 2010), 30 km north of Biscarrosse beach, and using a similar camera setting.

2.3. Storms

Wave data for this study were obtained from Wavewatch III model (Tolman, 1991) at the grid point facing the beach (1°30′W, 44°30′N, Fig. 1) in about 70-m water depth, at a 3-h interval over the study period (2007–2012). The significant wave height, Hs was further corrected via linear regression with a directional wave buoy (1°26.8′W, 44°39.15′N) moored in 50-m water depth, following Castelle et al. (2014).

The commonly used peak over threshold method (POT) is applied on Hs to select large wave conditions and identify storms (e.g. Dorsch et al., 2008). A 5–10% exceedance Hs is commonly adopted in scientific studies to define storm events (e.g. Dorsch et al., 2008; Rangel-Buitrago and Anfuso, 2011; Splinter et al., 2014a; Castelle et al., 2015). In the present work, Hs values with a probability of occurrence < 5% are considered as major storms, corresponding to an Hs of 3.68 m, also in line with Splinter et al. (2014a) and Castelle et al. (2015). A single storm is defined as a continuous period of Hs exceeding this threshold (Fig. 3) and lasting at least one tidal cycle (12 h), consistent with Senechal et al. (2015) approach and particularly to account for the impact of tide. Another key parameter used in the present analysis is the Storm intensity I (m^2hr), which is defined in several studies (e.g. Dolan and Davis, 1992; Karunarathna et al., 2014; Senechal et al., 2015) as the product of the maximum Hs by the storm duration, in line with annual maxima method. Here, we chose to follow the more time-integrated definition for I given by Mendoza et al. (2011), which is:

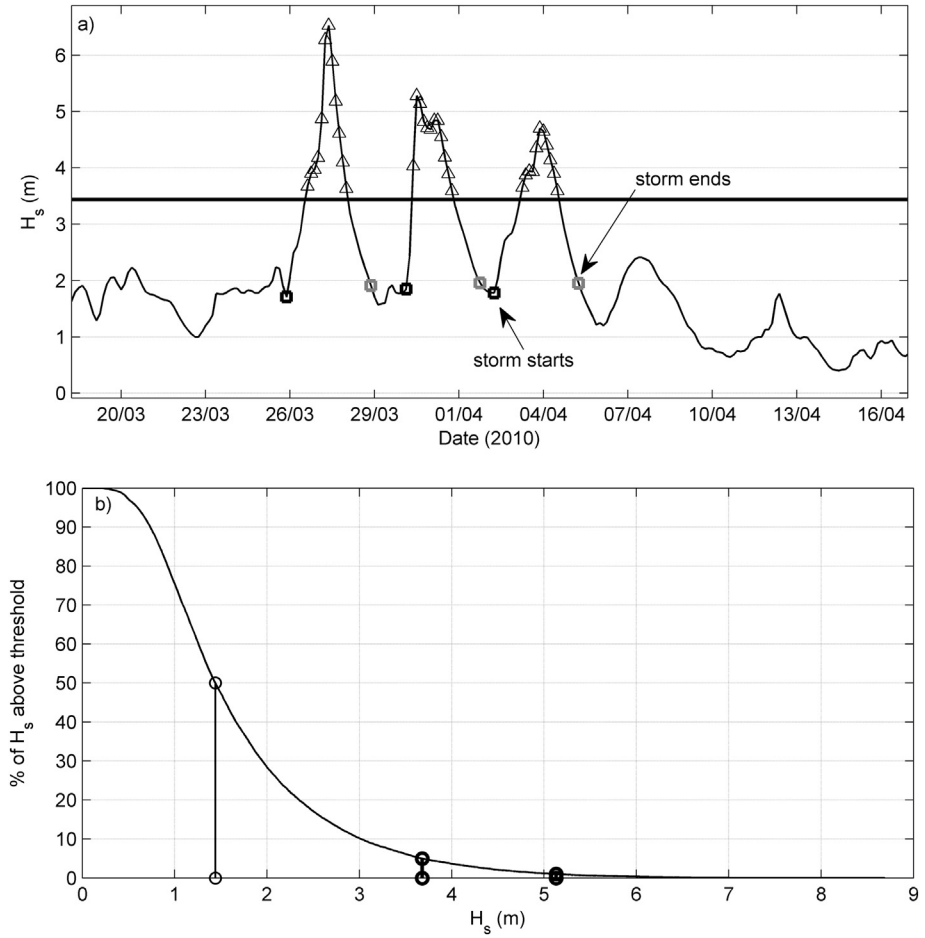

Fig. 3. Illustration of the method used to select a) storm characteristics, beginning and end of *Hs* above the threshold (*Hs* = 3.8 m, 95% exceedance level, shown as horizontal line in upper plot) and in b) the exceedance level where the 50, 95 and 99% levels are shown. In a), squares are the beginning and end of storms, triangular marks are values greater than the threshold.

$$I = \int_{t_1}^{t_2} H_s(t)^2 dt \tag{1}$$

where the storm duration D is the time between the beginning t_1 and the end t_2 of each storm. Initiation of a storm t_1 however was defined as the time when the three hourly-averaged *Hs* exceeded the 0.75 quantile (1.9 m), to be consistent with Masselink et al. (2014), and the end of the storm t_2 was the time when the three hourly-averaged *Hs* returned below 1.9 m (Fig. 3a).

2.4. Storm impact

The Storm impact $\Delta < X_{s,i} >$ (in meters) is estimated as the mean alongshore averaged cross-shore shoreline migration from the beginning to the end of each storm, equivalent to the end point rate method (Genz et al., 2007). There can be several ways to define the recovery duration after each storm. For example, Ranasinghe et al. (2012) used an approach based on the beach states, where the time the nearshore morphology takes to evolve from a post-storm state (e.g. dissipative/longshore bar and trough) to its modal state (i.e. the most frequently occurring beach state e.g. rhythmic bar and beach or transverse bar and rip) is defined as the recovery duration. In our study, the recovery duration T_r (in days) refers to the post-storm period of continuous accretion, at the end of which the beach is assumed stabilized. Daily average locations are determined from the shoreline location at the end of each storm. The length of the period of continuous accretion is determined by the number of days taken to reach the first maximum migration (recovery) value. This method contrasts with some existing methods (e.g. using beach state as in Ranasinghe et al., 2012) as it does not depend on any forcing parameter. However, the method is highly depended on the amount of shoreline recovery as considered in Corbella and Stretch (2012).

A multiple linear regression (Eq. (2)) is used to investigate the role of 5 forcing/modulating parameters on shoreline changes during storm ($\Delta < X_{s,i} >$) and on recovery periods (T_r): current storm energy I_i, previous storm influence, time between storms, tide range *TR* and sandbar-to-shoreline distance.

$$Y = co + \sum_{1}^{n} C_k Z_k + \varepsilon \tag{2}$$

where Y is the response variable, Z the predictor or causative variable, n is the number of events ($n = 36$), c_o and C_k are the non-standardized regression coefficients and ε is the residual term. Forcing terms are considered independent. The relative contribution $P(Z)$ of each forcing parameter is estimated from the ratio of individual variance to the total following Eq. (3):

$$P(Z) = 100\sqrt{\frac{S_k}{S_Y}}\ (k = 1, 2, \ldots 5) \tag{3}$$

where S_k is the variance of $C_k Z_k$ and S_Y is defined as the sum of variances of all causative components $S_Y = \sum_1^k C_n Z_n$ to insure a total of 100%.

The previous storm influence ($S < X_{s\text{-}i} >$) is defined as the rate of previous storm impact ($\Delta < X_{s\text{-}i} >$) with respect to the time interval (Δt in days) between storms (end of a storm and the start of another storm) based on the equilibrium concept that shoreline response depends on

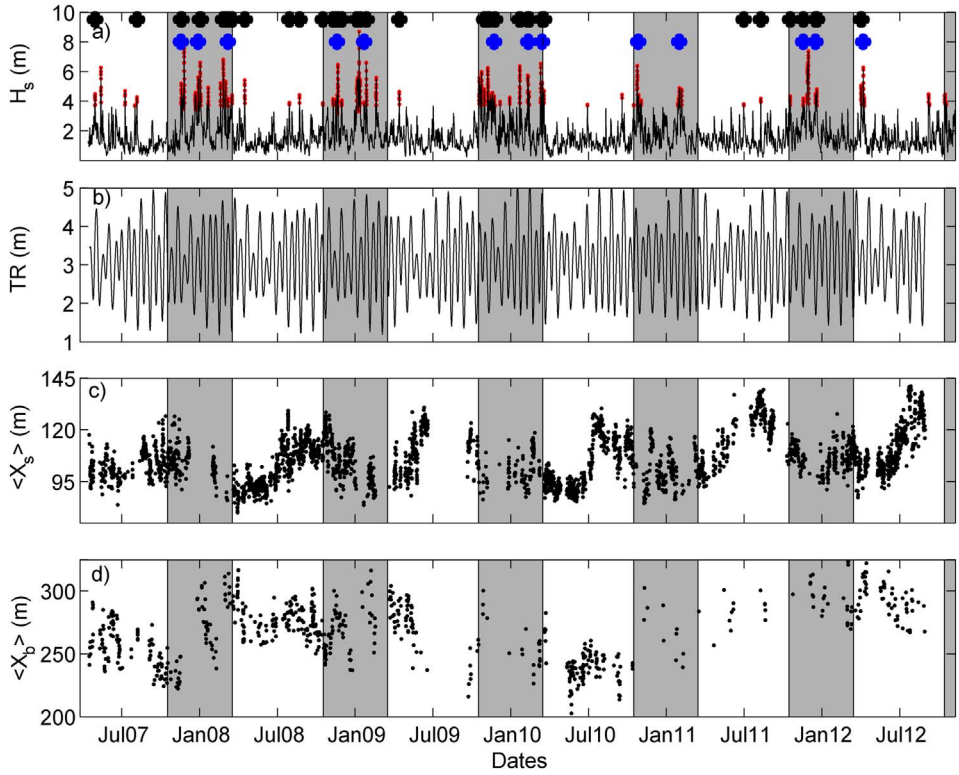

Fig. 4. Time series of a) significant wave height *Hs* with storm periods ($Hs > 3.68$ m) in dots, selected 36 storms are marked in large black dots and 13 clusters of storm are marked circles in gray, b) tidal range *TR* c) alongshore-averaged shoreline location $< X_s >$ and d) alongshore-averaged sandbar location $< X_b >$.

the antecedent beach state (Yates et al., 2009) as in Eq. (4):

$$S < X_{s-i} > = \frac{\Delta < X_{s-i} >}{\Delta t} \quad (4)$$

3. Results

Fig. 4a shows that wave regime has large seasonal variations, with low and high energy in summer and winter, respectively, with *Hs* ranging from < 1 m to 9 m. Fig. 4c shows that the alongshore-averaged shoreline location $< X_s >$ also follows a seasonal cycle with most onshore (85 m) and offshore (150 m) position in winter and summer, respectively. In Fig. 4d, the alongshore-averaged sandbar location $< X_b >$ shows a large variability (range of 110 m), varying between 212 m to 322 m with outermost location in winter and a less marked seasonal cycle. On average, the sandbar-to-shoreline distance $< X_b > - < X_s >$ is 162 m, but it can be larger (227 m) or smaller (102 m) during large (winter) and weak (summer) wave conditions, respectively.

3.1. Characteristics of individual storms and morphological impact

In total, 60 storms were identified during the 6-year study period. However, due to gaps in the video data, which precluded the derivation of shorelines, 24 of these storms were discarded from further analysis. The analysis presented herein therefore is based on the remaining 36 storms (Fig. 4a, marked black). The mean peak storm wave height is 4.9 m (standard deviation σ = 1.04 m) with the mean wave height throughout the storm duration being 4.5 m (σ = 0.8 m). The mean storm peak wave periods throughout all the storms is 12.15 s (σ = 2.16 s) and the mean storm duration 33 h (σ = 32 h).

The overall average interval between storms is predominantly seasonal (Fig. 5). Storms are more frequent in winter, while occurring almost throughout the year. In summer, only a few and short storms (< 6 h) are observed and usually do not meet the requirement of a complete tidal cycle (see Section 2.3). In winter (Table 1), 60% of storms recur within 10 days, while in summer this occurrence is observed to be sparse, with storms recurring on average within 100 days. The year 2011 recorded the lowest number of storms, with 9 storms causing only limited erosion. It is also seen that the standard deviation of storm energy is large in winter, which drives the temporality of the observed shoreline response (Fig. 5a, thin dot solid line) and sandbar (Fig. 5a, line marked circles). The largest number of storms and most extreme ($Hs > 5$ m, defined as the 99% percentile, Table 1) are observed in 2008 (25%), 2009 (25%) and 2010 (22%), which induced a large total erosion particularly in 2009 (Table 1). Individual storms result in a wide range of shoreline impacts (Table 1), from large erosion (− 21 m) and sometimes to accretion (+ 14 m). The immediate cause of this (uncommon) accretion during storms is unknown, but sediment input from dune erosion is one possible mechanism for upper beach accretion (van Gent et al., 2008). The mean storm impact on the shoreline throughout all storms is an erosion of 8.7 m (σ = 8.9 m).

3.2. Modulation of storm impact and recovery by previous events, tides and sandbar presence

Storm impact on the shoreline is often quantified separately from the influence of sandbars and tides, except for some recent attempts (e.g. Senechal et al., 2015; Stokes et al., 2015). Here, the relative contribution of the current and previous storms, tides and sandbars, are investigated together through a multiple linear regression (described in Section 2.4). Overall, Fig. 6a–b show that a good agreement is found between reconstructed and observed $\Delta < X_s >$ and T_r with regression coefficients equal to 0.74 and 0.69 (both significant at 95% level), respectively. Even though Table 2 shows that cross-correlation between terms of the multiple linear regression can be substantial (e.g. waves conditions vs. sandbar location) showing some physical links, where the values are low, the results can nonetheless be used with reasonable accuracy since they are significant at 95% confidence level. Fig. 6c–d

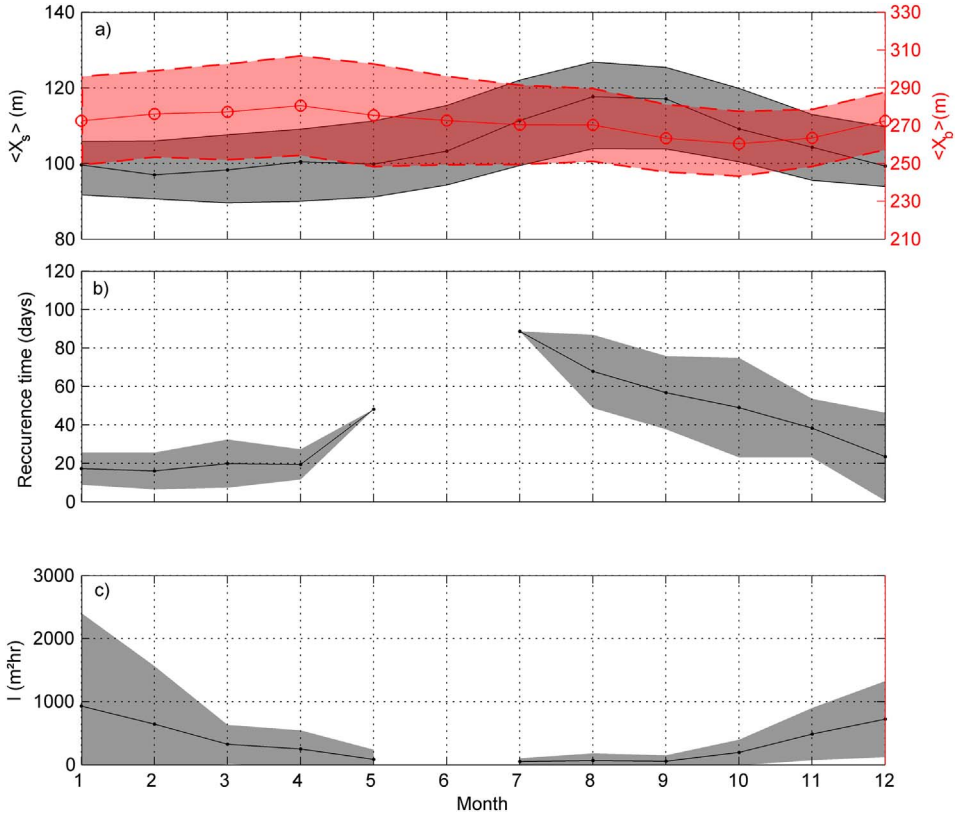

Fig. 5. Monthly-averaged characteristics of a) shoreline $< X_s >$, solid lines indicate monthly standard deviations and sandbar locations $< X_b >$, dash lines mark standard deviations; b) recurrence interval between storms; and c) average storm energy I (m^2hr) per month. Shaded areas around lines indicate the monthly standard deviation.

Table 1
Storm characteristics from 2007 to 2012 of maximum *Hs* (m), percentage (%) of extreme storms ($Hs > 5.0$ m, 99% threshold), annual average storm impact $\Delta < X_{s,i} >$ (m), and annual average storm duration (in days).

	Number of storms	Hs_{max} (m)	$Hs_{max} > 5$ m (%)	$\Delta < X_s >$ (m)	Duration (days)
2007	7	4.7	11	− 6.4	2.7
2008	18	5.0	25	− 8.0	3.4
2009	15	5.0	25	− 12.4	4.0
2010	13	4.7	22	− 6.5	2.5
2011	9	4.8	4	3.0	2.7
2012	11	4.5	11	− 10.3	4.5
mean	12	4.8	16	− 7.0	3.3

shows the contribution (in %) of each term on the total $\Delta < X_s >$ and T_r variance, together with their confidence level. Fig. 6c indicates that storm impact depends predominantly (55%) on current storm energy. It is a common outcome that wave conditions dominate the shoreline response during storms (e.g. Yates et al., 2009; Davidson et al., 2013; Castelle et al., 2015), with large intensities (i.e. *D* and/or *Hs*) resulting in large impacts on shoreline, but here we show that previous conditions have a substantial role (37%) while modulation by tide and sandbar play only a minor role (8% for tide and sandbar altogether). In contrast, during recovery (Fig. 6d), it is almost the reverse: while current and previous wave conditions have a secondary importance (15% and 13%, respectively), tide and sandbar contributions rise to 45 and 23%, respectively. This clearly shows a different forcing control on beach response between energetic, eroding conditions and recovery periods. This suggests that in times of low energy, shoreline retreat could be reduced, as was observed in 2011.

3.3. Storm sequences

Fig. 7 shows an ensemble-averaged analysis of the evolution of the sandbar and shoreline location during the post-storm recovery period. Fig. 7b shows that while wave height is decreasing after the storm, the shoreline continuously migrates offshore (3.7 m/day) before it reaches stabilization after 9 days (on average), which can be used as an average estimate for the post-storm recovery duration at Biscarrosse. This post-storm recovery duration is different from the time interval between storms; whereas the interval between storms could comprise both accretion and erosion, T_r is purely continuous accretion. Interestingly, while the shoreline is observed to stabilize in 9 days on average, the sandbar continuously migrates onshore under persistent moderate wave conditions, indicating a longer recovery but also a post-storm onshore migration that is likely to end up with the bar welding to the upper beach under persistent calm conditions, in line with downstate beach transition schemes (Wright and Short, 1984; Ranasinghe et al., 2004).

Based on this recovery duration, storm clusters are defined as a group of storms recurring in < 10 days. 13 such clusters are identified within the 6-year period, with at least one per year. The overall impact of clusters on shoreline location ranges from no substantial change to

Table 2
Cross-correlation coefficients between terms used in the multiple linear regression analysis for storm impact $\Delta < X_s >$ (upper white panel) and recovery T_r (lower gray panel) (Section 3.2).

	Waves	Previous conditions	Sandbar	Tide
Waves		0.09	−0.35	−0.24
Previous conditions	0.13		0.15	0.10
Sandbar	0.01	0.04		0.27
Tide	0.03	−0.13	−0.07	

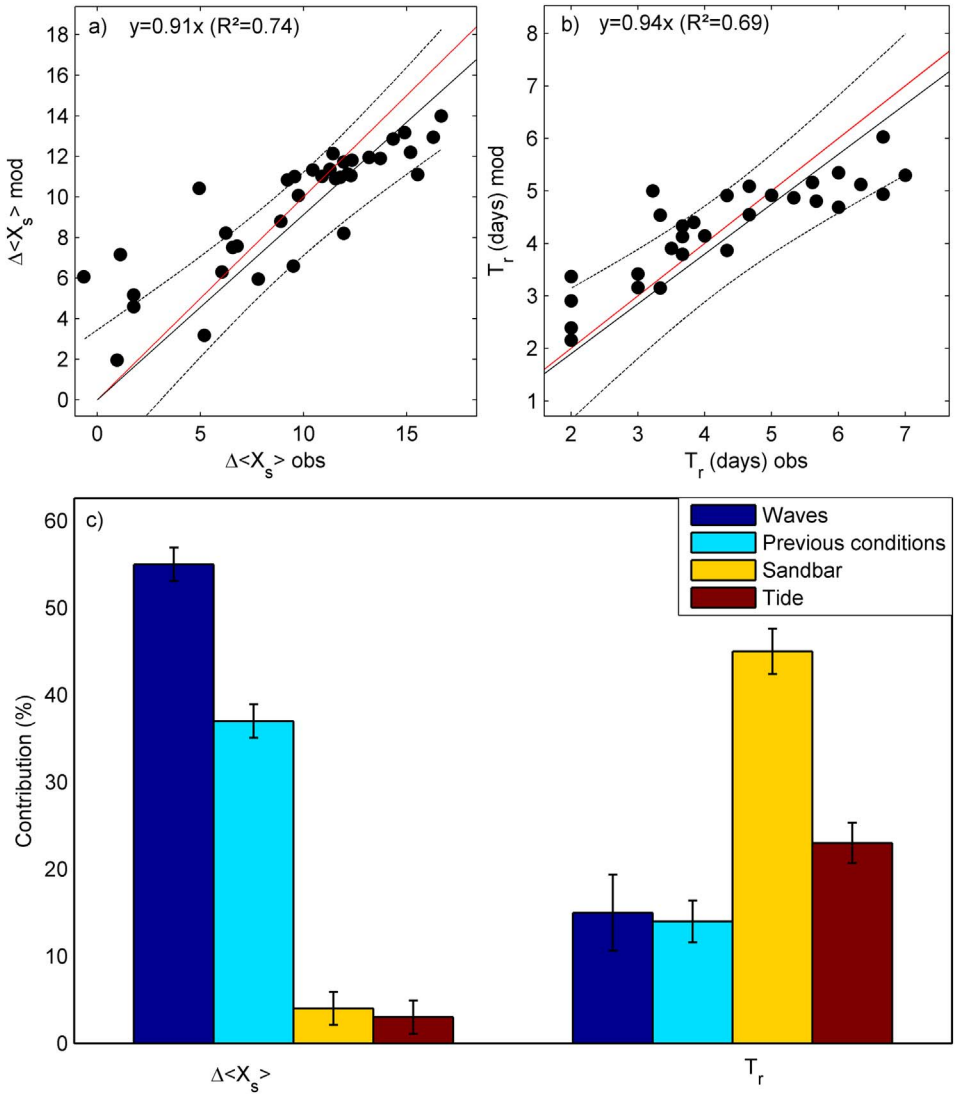

Fig. 6. Multiple linear regression analysis for $\Delta < X_s >$ (left) and T_r (right). a) and b) illustrate the comparison between observed and reconstructed variables. Thick solid and thin solid lines are 1:1 and linear regression (forced through the origin), respectively, while dashed lines indicate the 95% confidence levels. Lower panels c-d) describe the percentage of reconstructed signal explained by each component during storms and recovery, respectively. Error bars show the 95% confidence levels.

16 m of recession. The cluster with the largest number of storms observed in Nov–Dec 2009 with a total energy of 7133 m^2hr resulted in 14 m erosion. However, a smaller cluster of 2 events with a cumulative energy of 5573 m^2hr resulted in 11 m shoreline retreat, as this cluster includes the longest storm lasting 12 days in January 2009.

Fig. 8 shows the impact of storms $\Delta < X_s >$ ranked from one to five in the clusters. Note that the storm numbering here only depends on the occurrence sequence of the individual storms in the cluster, which means the first storm is not necessarily the most energetic. It is clear that the storm impact within a cluster decreases with storm rank. The influence of previous storms and the importance of recurrence is discussed in the next section.

4. Discussion

4.1. Role of sandbars and tides in modulating storm impact and recovery

Results in Section 3.2 (Fig. 6c) show that the influence of tide and sandbar during storms on the shoreline is not substantial in comparison with present storm intensity and previous storm influence. The influence of tide and sandbar contribute 8% in total. The influence of tide is not statistically significant (correlation coefficient < 0.1) and that of the sandbar, although statistically significant at the 95% confidence level, is weak (correlation coefficient ~ 0.2) in comparison to storm intensity and previous storm influence. Though it has been observed elsewhere (e.g. Robin et al., 2007; Davidson and Turner, 2009) that spring tides might enhance storm impact of the upper beach, it is hard to conclude with our dataset. The shoreline proxy used in this study could also have an impact on the contribution of the tides during storms. Similarly, the inner sandbar has only a limited influence on shoreline retreat, though one could expect that the closer the sandbar is to the shoreline, the more the inner sandbar will be coupled to the shoreline and plays its sheltering effect. For example, by limiting incoming wave height (Masselink et al., 2006; Davidson and Turner, 2009; Almar et al., 2010) through breaking over the shallow crest. This could result in large variability in the cross-shore shoreline location. Given that this is a double-barred beach, a coupling between the inner and outer sandbars could influence the effect of the inner bar on the shoreline. For the post-storm period, Fig. 6d shows that both tide and sandbar location affect substantially the recovery values T_r thereby modulating the recovery duration.

The use of a linear regression for possible non-linear relationships between the various parameters is foremost to identify the predominant parameters. To account for the linearity in the multiple regression

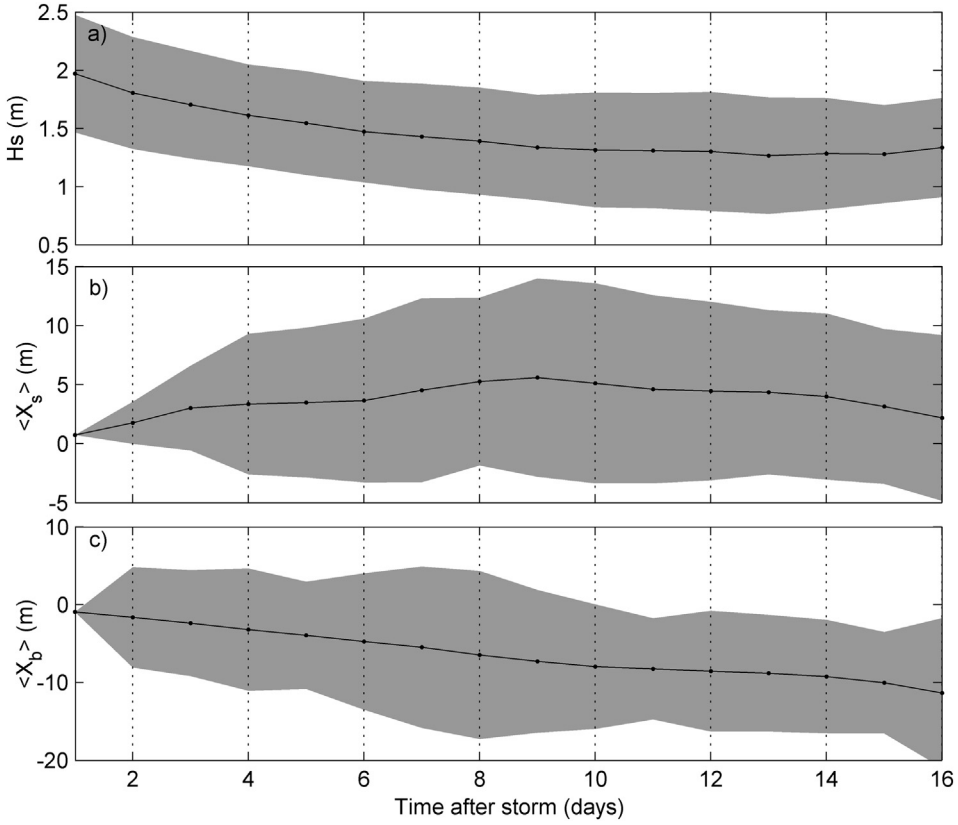

Fig. 7. Ensemble-averaged (over 36 storms) evolution during post-storm recovery period for a) *Hs*, b) shoreline location $< X_s >$ and c) sandbar location $< X_b >$ from their location at the end of the storm. Shaded zone stands for standard deviation.

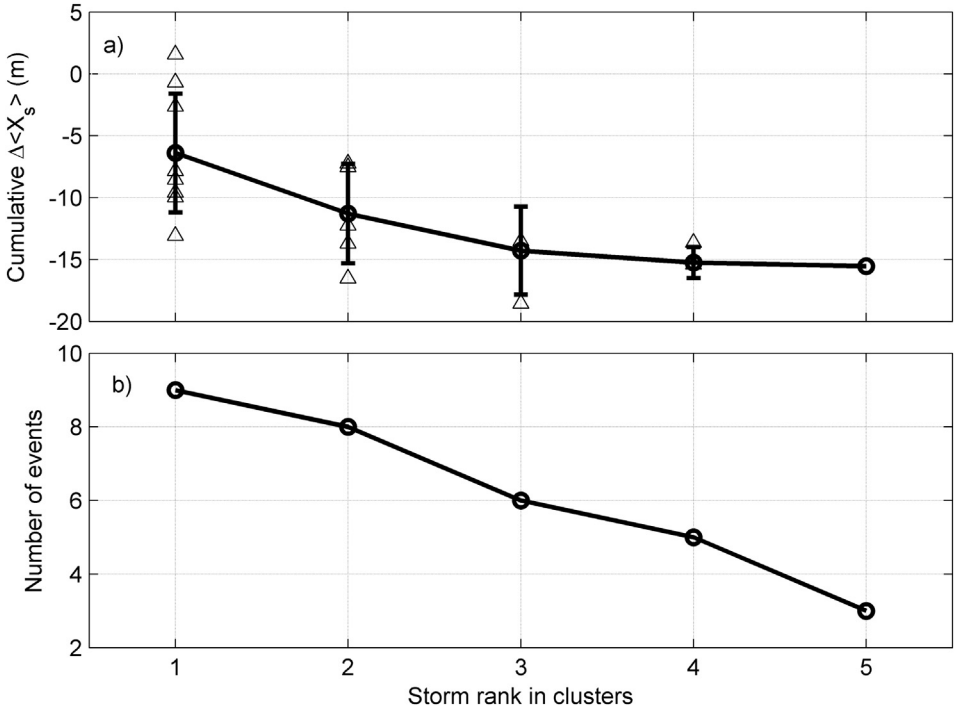

Fig. 8. Cluster of storms. a) Cumulative storm impact and b) number of storms taken into account as a function of their rank in the cluster. Circles and triangles in a) illustrate average and individual values, respectively. In a) offshore direction is traced by more positive values.

method used, several parameters were tested including the relative tide range ($RTR = TR/Hs$) and hydrodynamic forcing index (HFI, Almar et al., 2010). As the RTR increases, wave action becomes strongly controlled by tidal level and sandbar location, or most probably a combination of both. Under such moderate wave conditions, a large tidal range will result in reducing the occurrence of surf-zone processes at the upper beach, and thus increase recovery duration. It will also change the breaking intensity and occurrence over the bar which can have a direct consequence on the fine threshold between erosion/accretion and no change, as observed by Almar et al. (2010). Stokes et al. (2015) observed that at seasonal scale, the inclusion of tide (through a modulation of incoming wave energy) improves the prediction of shoreline change, and it is expected to even be truer at short/event time scales, in particular the post-storm relaxation time. This is mainly due to the modulation of swash characteristics by tide, as observed by Guedes et al. (2011).

4.2. Frequency of recurrence of storms and shoreline resilience

The fact that previous storm influence contributes significantly to shoreline change, underlines the significance of the so-called beach memory effect (e.g. Turki et al., 2012; Reeve et al., 2014) where shoreline response to events depends on the history of beach conditions (e.g. see Splinter et al., 2014a). In line with previous studies (Yates et al., 2009; Castelle et al., 2014; Angnuureng, 2016), the first winter storms drive the most pronounced erosion because the wave energy disequilibrium and erosion potential are large. During the rest of winter season, even if the beach is often exposed to severe storms, they do not significantly erode the beach as the disequilibrium energy is smaller. It should be noted that the correlation coefficient between the preceding storm influence and storm impact was observed to be negative (-0.35, significant at the 95% level), which means that if the previous storm event is larger but closer to the current storm event, the erosion will be less. If storm recurrence is long enough, individual storm impacts become independent as the beach has time to recover and reach its pre-storm equilibrium. If the interval is sufficiently short, such as for storms in sequences described in Section 3.3, only the previous storm appears to have a destabilizing effect on the beach while the subsequent storms decreasingly impact on the beach. This is consistent with Dissanayake et al. (2015) who found at Formby Beach (UK) that the largest erosion was always observed for the first storm, because the beach had sufficient time to recover fully from the previous storm season.

Our observations are in line with Coco et al. (2014) and Splinter et al. (2014a) who demonstrated that a sequence of storms does not necessarily result in cumulative erosion, although frequent sequences can slightly affect shoreline resilience (Dissanayake et al., 2015). These results suggest a possible relation between beach changes on episodic and seasonal timescales, and that the frequency of storm recurrence and the storm frequency change over time (e.g. seasonal, interannual, climate change) are of some importance in assessing beach equilibrium and evolution. When storm sequences are frequent in winter, only the first storm causes severe impact while the rest of the storms in the sequence have minimal effect. Considering variable recurrence frequency, longer storm intervals enhance storm impact. Storm impact will also change if the frequency of storms (i.e. storminess) evolves under changing climate, or under regional modes of climate variability (e.g. on the west coast of Europe the North Atlantic Oscillation, NAO; northward of 52°N (Hurrell, 1995), and the West Europe Pressure Anomaly, WEPA, southwards of 52°N (Castelle et al., 2017)). Such natural modes of climate variability can cause outstanding series of storm events such as that observed during the 2013/2014 winter in Western Europe (Masselink et al., 2016), and drive some interannual change in beach and sandbar behavior (Masselink et al., 2014). It is hypothesized that our findings on the timescale of storms may apply to the interannual timescales, where a winter with extreme storminess following a few years of reasonably fair winter wave conditions may maximize coastal erosion at the scale of a winter season. This is what was observed along the west coast of Europe during the 2013/2014 winter along the west coast of Europe (Masselink et al., 2016) and during the highest WEPA index recorded over at least the last 75 years (Castelle et al., 2017), and more recently during the 2015/2016 winter along the west coast of the US for one of the largest El Nino over the last 145 years (Barnard et al., 2017).

5. Conclusions

Six years of video-derived shoreline and sandbar locations were collected at the meso- to macrotidal barred beach of Biscarrosse, SW France. Over 60 individual storms (~15 storms per year) were identified using 5% exceedance for Hs ($Hs > 3.68$ m) as the storm threshold. However, due to the non-existence of shoreline data during 24 of these storms because of poor weather and video malfunctions, only the remaining 36 storms were investigated in detail. Based on these, the average storm recurrence is 27 days in winter, with 60% of the storms recurring within 10 days. This large recurrence shows a strong seasonality in storm occurrence, also reflected in the shoreline and sandbar locations. Shoreline retreat is predominantly influenced by the current storm (55%), but the previous storm influence also plays a significant role (37%). The modulating parameters such as the sandbar-to-shoreline distance and tides play only a secondary role (8%) in storm induced shoreline retreat. Antecedent storm conditions were also observed to reduce current storm impact, likely explained by the rapid adjustment of the beach to a more energetic state when a storm occurs.

With moderate wave energy during post-storm recovery, the influence of the tidal range and the sandbar increases (23 and 45%, respectively), with recovery duration increasing for larger tidal range and larger distance between the sandbar and the shoreline. The presence of a double sandbar on the meso- to macrotidal Biscarrosse beach induces a threshold on wave energy (Almar et al., 2010) at the shore by height limitation due to breaking over the sandbar which modifies onshore wave energy and frequencies: the magnitude of shoreline change may be highly controlled by the conjugate effect of sandbar and tide. These results argue in favor of integrating sandbar and tide effects in shoreline equilibrium models, especially the way in which they influence the complex beach recovery process, which could substantially improve model performance at longer timescales.

Analysis of post-storm beach recovery shows that the beach recovers within 9 days of individual storms. With respect to storm clusters, the first storms result in the highest erosion. This agrees with equilibrium-based approaches where storms are less and less effective in eroding the beach as the beach progressively reaches a new equilibrium with the prevailing wave conditions. The beach response depends on the beach 'memory'. These results suggest the existence of beach resilience interactions at different timescales. Beach resilience is weaker when storms are infrequent (in summer) and vice versa in winter. These results also show that a weaker single storm could have a larger impact than stronger storm occurring in the middle of storm sequence, illustrating the key role of the temporal evolution of not only the storm intensity but also their frequency of recurrence when considering beach resilience.

Acknowledgements

The first author is co-funded by SCAC (French embassy in Ghana) and ARTS-IRD programs. Authors acknowledge the Region Aquitaine for financially supporting the installation of the video system at Biscarrosse. This research has received support from French grant through ANR COASTVAR: ANR-14-ASTR-0019. RR is supported by the AXA Research fund and the Deltares Harbour, Coastal and Offshore Engineering Research Programme *'Bouwen aan de Kust'*. BB is supported by French "Agence Nationale de la Recherche" through project CHIPO (ANR-14-ASTR-0004-01).

References

Aarninkhof, S.G.J., Turner, I.L., Dronkers, T.D.T., Caljouw, M., Nipius, L., 2003. A video-based technique for mapping intertidal beach bathymetry. Coast. Eng. 49 (4), 275–289.

Almar, R., Castelle, B., Ruessink, B.G., Senechal, N., Bonneton, P., Marieu, V., 2009. High-frequency video observation of two nearby double-barred beaches under high-energy wave forcing. J. Coast. Res. SI 56 (2), 1706–1710.

Almar, R., Castelle, B., Ruessink, G., Senechal, N., Bonneton, P., Marieu, V., 2010. Two and three-dimensional double-sandbar system behaviour under intense wave forcing and a meso–macro tidal range. Cont. Shelf Res. 30 (7), 781–792.

Angnuureng, D.B., 2016. Shoreline Response to Multiscale Oceanic Forcing from Video Imagery. (PhD thesis) Université de Bordeaux (181 pp.).

Ba, A., Senechal, N., 2013. Extreme winter storm versus summer storm: morphological impact on a sandy beach. J. Coast. Res. SI 65, 648–653.

Barnard, P.L., Hoover, D., Hubbard, D.M., Snyder, A., Ludka, B.C., Kaminsky, G.M., Ruggiero, P., Gallien, T., Gabel, L., McCandless, D., Weiner, H.M., Cohn, N., Anderson, D.L., Serafin, K.A., 2017. Extreme oceanographic forcing and coastal response due to the 2015-2016 el Niño. Nat. Commun. 8, 14365.

Birrien, F., Castelle, B., Dailloux, D., Marieu, V., Rihouey, D., Price, T.D., 2013. Video observation of megacusp evolution along a high-energy engineered sandy beach: Anglet, SW France. J. Coast. Res. SI 65, 1727–1732.

Boak, E.H., Turner, I.L., 2005. Shoreline definition and detection: a review. J. Coast. Res. 21 (4), 688–703.

Butel, R., Dupuis, H., Bonneton, P., 2002. Spatial variability of wave conditions on the French Aquitanian coast using in-situ data. J. Coast. Res. SI 36, 96–108.

Castelle, B., Bonneton, P., Dupuis, H., Senechal, N., 2007a. Double bar beach dynamics on the high-energy meso-macrotidal French Aquitanian coast : a review. Mar. Geol. 245, 141–159.

Castelle, B., Turner, I.L., Ruessink, B.G., Tomlinson, R.B., 2007b. Impact of storms on beach erosion: Broadbeach (Gold Coast, Australia). J. Coast. Res. SI 50, 534–539.

Castelle, B., Marieu, V., Bujan, S., Ferreira, S., Parisot, J.P., Capo, S., Senechal, N., Chouzenoux, T., 2014. Equilibrium shoreline modelling of a high energy meso-macro-tidal multiple-barred beach. Mar. Geol. 347, 85–94.

Castelle, B., Marieu, V., Bujan, S., Splinter, K.D., Robinet, A., Senechal, N., Ferreira, S., 2015. Impact of the winter 2013-2014 series of severe Western Europe storms on a double-barred sandy coast: beach and dune erosion and mega cusp embayments. Geomorphology 238, 135–148.

Castelle, B., Dodet, G., Masselink, G., Scott, T., 2017. A new climate index controlling winter wave activity along the Atlantic coast of Europe: the West Europe pressure anomaly. Geophys. Res. Lett. 44. http://dx.doi.org/10.1002/2016GL072379.

Coco, G., Senechal, N., Rejas, A., Bryan, K.R., Capo, S., Parisot, J.P., Brown, J.A., MacMahan, J.H.M., 2014. Beach response to a sequence of extreme storms. Geomorphology 204, 493–501.

Corbella, S., Stretch, D.D., 2012. Shoreline recovery from storms on the east coast of southern Africa. Nat. Hazards Earth Syst. Sci. 12, 11–22.

Davidson, M.A., Turner, I.L., 2009. A behavioral template beach profile model for predicting seasonal to interannual shoreline. J. Geophys. Res. 114, F01020. http://dx.doi.org/10.1029/2007JF000888.

Davidson, M.A., O'Hare, T.J., George, K.J., 2008. Tidal modulation of incident Wave Heights: fact or fiction? J. Coast. Res. 24 (2), 151–159.

Davidson, M.A., Splinter, K.D., Turner, I.L., 2013. A simple equilibrium model for predicting shoreline change. Coast. Eng. 73, 191–202.

Davis, R.A., 1985. Beach and nearshore zone. In: DAVIS, R.A. (Ed.), Coastal Sedimentary Environments. Springer-Verlag, New York, pp. 379–444.

Dissanayake, P., Brown, J., Karunarathna, H., 2015. Impacts of storm chronology on the morphological changes of the Formby beach and dune system, UK. Nat. Hazards Earth Syst. Sci. 15, 1533–1543.

Dolan, R., Davis, R., 1992. An intensity scale for Atlantic coast northeast storms. J. Coast. Res. 8 (4), 840–853.

Dorsch, W., Newland, T., Tassone, D., Tymons, S., Walker, D., 2008. A statistical approach to modeling the temporal patterns of ocean storms. J. Coast. Res. 24 (6), 1430–1438.

Douglas, B.C., Crowell, M., 2000. Long-term shoreline position prediction and error propagation. J. Coast. Res. 16 (1), 145–152.

Fenster, M.S., Dolan, R., Morton, R.A., 2001. Coastal storms and shoreline change: signal or noise? J. Coast. Res. 17 (3), 714–720.

Ferreira, O., 2005. Storm groups versus extreme single storms: predicted erosion and management consequences. J. Coast. Res. SI 42, 221–227.

Flater, D., 2010. www.wXtide32.com (Last accessed on 25/01/2016).

Frazer, L.N., Anderson, T.R., Fletcher, C.H., 2009. Modeling storms improves estimates of long-term shoreline change. Geophys. Res. Lett. 36, L20404.

Gallagher, E.L., Elgar, S., Guza, R.T., 1998. Observations of sandbar evolution on a natural beach. J. Geophys. Res. 103, 3203–3215.

Gallagher, E.L., MacMahan, J.H., Reniers, A.J.H.M., Brown, J., Thornton, E.B., 2011. Grain size variability on a rip channeled beach. Mar. Geol. 287, 43–53.

Genz, A.S., Fletcher, C.H., Dunn, R.A., Frazer, L.N., Rooney, J.J., 2007. The predictive accuracy of shoreline changes rate methods and alongshore beach variation on Maui, Hawaii. J. Coast. Res. 23 (1), 87–105.

Grasso, F., Michallet, H., Barthélemy, E., Certain, R., 2009. Physical modeling of intermediate cross-shore beach morphology: transients and equilibrium states. J. Geophys. Res. 114, C09001.

Guedes, R.M.C., Calliari, L.J., Holland, K.T., Plant, N.G., Pereira, P.S., Alves, F.N.A., 2011. Short-term sandbar variability based on video imagery: comparison between time–average and time–variance techniques. Mar. Geo. 289, 122–134.

Hansen, J.E., Barnard, P.L., 2010. Sub-weekly to interannual variability of a high-energy shoreline. Coast. Eng. 57, 959–972.

Holland, K.T., Holman, R.A., Lippmann, T.C., 1997. Practical use of video imagery in nearshore oceanographic field studies. IEEE J. Ocean. Eng. 22 (1), 81–92.

Holman, R., Haller, M., 2013. Remote sensing of the nearshore. Annu. Rev. Mar. Sci. 113, 5–95.

Holman, R.A., Stanley, J., 2007. The history and technical capabilities of Argus. Coast. Eng. 54, 477–491.

Holman, R.A., Sallenger, A.H., Lippmann, T.C., Haines, J.W., 1993. The application of video image processing to the study of nearshore processes. Oceanography 6, 3.

Hurrell, J.W., 1995. Decadal trends in the North Atlantic oscillation: regional temperatures and precipitation. Science 269 (5224), 676–679.

Karunarathna, H., Pender, D., Ranasinghe, R., Short, A.D., Reeve, D.E., 2014. The effects of storm clustering on beach profile variability. Mar. Geol. 348, 103–112.

Lippmann, T.C., Holman, R.A., 1989. Quantification of sandbar morphology: a video technique based on wave dissipation. J. Geophys. Res. 94, 995–1011.

Lippmann, T., Holman, R., 1990. The spatial and temporal variability of sandbar morphology. J. Geophys. Res. 95, 11575–11590.

Madsen, A.J., Plant, N.G., 2001. Intertidal beach slope predictions compared to field data. Mar. Geol. 173, 121–139.

Maspataud, A., Ruz, M.-H., Hequette, A., 2009. Spatial variability in post-storm beach recovery along a macrotidal barred beach, southern North Sea. J. Coast. Res. 56, 88–92.

Masselink, G., Short, A.D., 1993. The effect of tide range on beach morphodynamics and morphology: a conceptual beach model. J. Coast. Res. 9 (3), 785–800.

Masselink, G., Kroon, A., Davidson-Arnott, R.G.D., 2006. Morphodynamics of intertidal bars in wave-dominated coastal settings-a review. Geomorphology 73, 33–49.

Masselink, G., Austin, M., Scott, T., Poate, T., Russell, P., 2014. Role of wave forcing, storms and NAO in outer bar dynamics on a high-energy, macro-tidal beach. Geomorphology 226, 76–93.

Masselink, G., Castelle, B., Scott, T., Dodet, G., Suanez, S., Jackson, D., Floc'h, F., 2016. Extreme wave activity during 2013/2014 winter and morphological impacts along the Atlantic Coast of Europe. Geophys. Res. Lett. 43 (5), 2135–2143.

Mendoza, E.T., Jimenez, J.A., Mateo, J., 2011. A coastal storms intensity scale for the Catalan sea (NW Mediterranean). Nat. Hazards Earth Syst. Sci. 11, 2453–2462.

Morton, R.A., Leacht, M.P., Painet, J.G., Cardozat, M.A., 1993. Monitoring beach changes using GPS surveying techniques. J. Coast. Res. 9 (3), 702–720.

Pape, L., Ruessink, B.G., 2008. Multivariate analysis of nonlinearity in sandbar behavior. Nonlinear Process. Geophys. 15, 145–158.

Peron, C., Senechal, N., 2011. Dynamic of a meso to macro-tidal double barred beach: inner bar response. J. Coast. Res. SI 64, 120–124.

Pianca, C., Holman, R., Siegle, E., 2015. Shoreline variability from days to decades: results of long-term video imaging. J. Geophys. Res. Oceans 120, 2159–2178. http://dx.doi.org/10.1002/2014JC010329.

Plant, N.G., Holman, R.A., 1997. Intertidal beach profile estimation using video images. Mar. Geol. 140, 1–24.

Plant, N., Holman, R., 1998. Extracting morphologic information from field data. Coast. Eng. Proc. 1 (26). http://dx.doi.org/10.9753/icce.v26.

Plant, N.G., Aarninkhof, S.G.J., Turner, I.L., Kingston, K.S., 2007. The performance of shoreline detection models applied to video imagery. J. Coast. Res. 23 (3), 658–670.

Ranasinghe, R., Symonds, G., Black, K., Holman, R., 2004. Morphodynamics of intermediate beaches: a video imaging and numerical modelling study. Coast. Eng. 51, 629–655.

Ranasinghe, R., Holman, R., de Schipper, M.A., Lippmann, T., Wehof, J., Minh Duong, T., Roelvink, D., Stive, M.J.F., 2012. Quantification of nearshore morphological recovery time scales using Argus video imaging: Palm Beach, Sydney and Duck, NC. Coast. Eng. Proc. 1 (33), 24.

Rangel-Buitrago, N., Anfuso, G., 2011. An application of Dolan and Davis (1992) classification to coastal storms in SW Spanish littoral. In: J. Coast. Res., SI64 (Proceedings of the 11th International Coastal Symposium), Szczecin, Poland, pp. 0749-0208.

Reeve, D.E., Pedrozo-Acuña, A., Spivack, M., 2014. Beach memory and ensemble prediction of shoreline evolution near a groyne. Coast. Eng. 86, 77–87.

Robin, N., Levoy, F., Monfort, O., 2007. Bar morphodynamic behaviour on the ebb delta of a macrotidal inlet (Normandy, France). J. Coast. Res. 23 (6), 1370–1378 (West Palm Beach (Florida), ISSN 0749–0208).

Senechal, N., Coco, G., Castelle, B., Marieu, V., 2015. Storm impact on the seasonal shoreline dynamics of a meso- to macrotidal open sandy beach (Biscarrosse, France). Geomorphology 228, 448–461.

Smit, M.W.J., Aarnikhof, S.G.J., Wijberg, K.M., Gozalez, M., Kingston, K.S., Southgate, H.N., Ruessink, G., Holman, R.A., Siegle, E., Davidson, M., Medina, R., 2007. The role of video imagery in predicting daily to monthly coastal evolution. Coast. Eng. 54, 539–553.

Splinter, K.D., Carley, J.T., Golshani, A., Tomlinson, R., 2014a. A relationship to describe the cumulative impact of storm clusters on beach erosion. Coast. Eng. 83, 49–55.

Splinter, K.D., Turner, I.L., Davidson, D.A., Barnard, P., Castelle, B., Oltman-Shay, J., 2014b. A generalized equilibrium model for predicting daily to inter-annual shoreline response. J. Geophys. Res. Earth Surf. 119, 1936–1958.

Stockdon, H.F., Holman, R.A., Howd, P.A., Sallenger, A.H., 2006. Empirical parameterization of setup, swash and runup. Coast. Eng. 53, 573–588.

Stokes, C., Davidson, M., Russell, P., 2015. Observation and prediction of three-dimensional morphology at a high-energy macrotidal beach. Geomorphology 243, 1–13.

Thornton, E.B., MacMahan, J.H., Sallenger Jr., A.H., 2007. Rip currents, mega-cusps, and eroding dunes. Mar. Geol. 240, 151–167.

Tolman, H.L., 1991. A third generation model for wind waves on slowly varying, unsteady and inhomogeneous depths and currents. J. Phys. Oceanogr. 21, 782–797.

Turki, I., Medina, R., Gonzalez, M., 2012. Beach memory. In: McKee Smith, Jane (Ed.), Proceedings of the 33rd International Conference, World Scientific, Santander, Spain, .

Turner, I., Leyden, V., Symonds, G., McGrath, J., Jackson, A., Jancar, T., Aarninkhof, S., Elshoff, I., 2001. Comparison of observed and predicted coastline changes at the Gold Coast artificial (surfing) reef, Sydney, Australia. In: Proceedings of International Conf. on Coast. Eng., Sydney, .

van de Lageweg, W.I., Bryan, K.R., Coco, G., Ruessink, B.G., 2013. Observations of shoreline–sandbar coupling on an embayed beach. Mar. Geol. 344, 101–114.

van Enckevort, I.M.J., Ruessink, B.G., 2001. Effect of hydrodynamics and bathymetry on video estimates of nearshore sandbar position. J. Geophys. Res. 106 (C8), 16969–16979.

van Gent, M.R.A., van Thiel de Vries, J.S.M., Coeveld, E.M., de Vroeg, J.H., Van de Graaff, J., 2008. Large-scale dune erosion tests to study the influence of wave periods. Coast. Eng. 55, 1041–1051.

Wright, L.D., Short, A.D., 1984. Morphodynamic variability of surf zones and beaches: a synthesis. Mar. Geol. 56, 93–118.

Wright, L.D., Short, A.D., Green, M.O., 1985. Short-term changes in the morphodynamic states of beaches and surf zones: an empirical predictive model. Mar. Geol. 62, 339–364.

Yates, M.L., Guza, R.T., O'Reilly, W.C., 2009. Equilibrium shoreline response: observations and modeling. J. Geophys. Res. 114.

Zhang, K., Douglas, B., Leatherman, S., 2002. Do storms cause long-term beach erosion along the U.S. east barrier coast? J. Geol. 110 (4), 493–502.